PHYSICAL REVIEW D **73,** 122004 (2006)

Adaptive filters for detection of gravitational waves from coalescing binaries

Antonio Eleuteri, Leopoldo Milano, Rosario De Rosa, and Fabio Garufi
Dip. di Scienze Fisiche, Università di Napoli "Federico II", via Cintia, I-80126 Napoli, Italia
and INFN sez. Napoli, via Cintia, I-80126 Napoli, Italia

Fausto Acernese and Fabrizio Barone
Dip. di Scienze Farmaceutiche, Università di Salerno, via Ponte Don Melillo, 84084 Fisciano (SA), Italia
and INFN sez. Napoli, via Cintia, I-80126 Napoli, Italia

Lara Giordano and Silvio Pardi
Dip. di Matematica ed Applicazioni, Universita di Napoli "Federico II", via Cintia, I-80126 Napoli, Italia
and INFN sez. Napoli, via Cintia, I-80126 Napoli, Italia
(Received 22 September 2005; published 20 June 2006)

In this work we propose use of infinite impulse response adaptive line enhancer (IIR ALE) filters for detection of gravitational waves from coalescing binaries. We extend our previous work and define an adaptive matched filter structure. Filter performance is analyzed in terms of the tracking capability and determination of filter parameters. Furthermore, following the Neyman-Pearson strategy, receiver operating characteristics are derived, with closedform expressions for detection threshold, false alarm, and detection probability. Extensive tests demonstrate the effectiveness of adaptive filters both in terms of small computational cost and robustness.

DOI: 10.1103/PhysRevD.73.122004 PACS numbers: 04.80.Nn, 05.40.Ca, 07.05.Kf, 07.60.Ly

I. INTRODUCTION

Gravitational wave (hereafter GW) detection is certainly one of the most challenging goals for today's physics: it represents a very strong proof in favor of the Einstein general relativity description of phenomena related to the dynamics of gravitation and the opening of a completely new channel of information on astrophysical objects [1–3]. Ground and space-based detectors are now operational or will be operational in the next years, with different bandwidths and sensitivities. The VIRGO/LIGO/GEO/TAMA ([4–7]) network of ground-based kilometer-scale laser interferometer gravitational wave detectors will probably be the key to open up a new astronomical channel of information in the frequency band 10 Hz to 10 kHz. In addition, when the proposed 5×10^6 kilometers long space-based interferometer LISA [8] will fly, another window will be opened in the frequency band $10^{-5} \div 1$ Hz. The sensitivities of the operational interferometers are becoming very interesting, producing reasonable hopes in the researchers that the first detection of gravitational waves is becoming very close.

Starting from the estimate of the huge computational cost of the data analysis for VIRGO/LIGO/GEO/TAMA (correlation with $10^5 \div 10^7$ templates), we decided to explore approaches able to reduce the computational cost of the overall search procedure. We devised an adaptive filter to be used as a first level trigger, to select interesting data blocks to be further analyzed with more refined optimal techniques based on matched filters. Our efforts were aimed at the implementation of a rough analysis with the following characteristics: small signal losses with respect to the use of matched filters, robustness against false detection, and low computational cost (for real-time execution).

Finally, considering that the algorithm does not require the knowledge of templates, it can be effectively used not only for the inspiral phase, but for the whole coalescence process. On the other hand if we want to implement a trigger running in real time, algorithms like IIR ALE, as we shall see, could be very useful. Despite the need of data whitening the algorithm can be used to set up a veto on false detection in the output of detection algorithms (such as a matched filter bank).

The main idea is to use the adaptive IIR ALE filter to "reconstruct" at its output the coherent component (if any) at its input. If the filter is correctly tracking the signal, the reconstruction consists of a noisy replica of the input coherent components. If we view the reconstruction as a *noisy template*, then a correlator detector can be built, which matches the raw filter input with its output. It should be noted that adaptivity of the filter is fundamental, since it allows the reconstruction of signals with a time varying frequency component. Therefore, the correlator "integrates" the local information obtained by the adaptive filter step-by-step.

The outline of the paper is the following. In Sec. II we define the signal model to which our analysis applies. In Sec. III we introduce the class of IIR ALE filters and describe their statistical properties in terms of impulse response and correlation functions; here we lay the ground for the developments in Sec. IV, where we describe the proposed adaptive correlator detector structure and formally derive the detection statistic distribution. In Sec. V

we show the performance of the filter in white, colored, and nonstationary noise environments. In the appendices we show the mathematical details of the detector statistics.

It should be noted that this work is an extension of previously published works [9,10].

II. SIGNAL MODEL

To establish the signal models, to use for our simulations, we will recall the up-to-date results of the theoretical studies on the last fate of a binary system constituted either of two neutron stars or two black holes. The theoretical investigations are performed dividing the coalescence event in three main distinct phases [11]:

(i) Adiabatic inspiral phase;
(ii) Merger phase;
(iii) Ring-down phase.

During the adiabatic inspiral phase, the time scale of the gravitational radiation reaction is much longer than the orbital period. The distance between the two compact objects composing the binary is large enough to consider their dimensions negligible (point masses hypothesis).

Near the end of the inspiral phase, the system evolves towards a dynamic instability, passing from a radiation reaction regime to a free-falling plunge, up to the final merging (the merger phase). This phase constitutes one of the most challenging problems for numerical relativity and is of concern for the experimentalist due to the lack of credited templates for matched filtering. Suitable templates for the binary black hole merger phase are the objective of current research (see e.g. [12,13] and references therein). The nonlinear phase of merging gradually goes towards a stationary regime that can be described as oscillations of this final newborn compact object (BH/NS) quasinormal modes. The emitted gravitational waves are described by the superposition of exponential damped sinusoids and carry information about the mass and the spin (see e.g. [14] for nonspinning binaries or [15,16] for spinning binaries) of the final newborn compact object (the ring-down phase).

From this evolutionary picture it is clear that the phases for which credited templates exist are the inspiral and ring-down phases, while for the merger phase, interesting results on suitable classes of templates are coming from recent numerical relativity studies. In Fig. 1 some examples of foreseen waveforms (called chirp) are shown during the inspiral phase of either neutron star binaries or black bole (hereinafter BH) of their process of coalescence.

In our analysis we consider the inspiral phase of coalescence, and so, for the sake of simplicity, we can assume a locally sinusoidal, amplitude and frequency modulated signal model. The chirp waveform is an example of such signals:

$$s(t) = a(t)\cos\psi(t), \tag{1}$$

where $a(t)$ and $\psi(t)$ are monotone, slowly growing power laws. Defining a slowly varying pseudoperiod as $T(t) = 2\pi/\dot{\psi}(t)$, if $a(t)$ has small relative changes over the pseudoperiod, then an adaptive scheme can be devised to track such a signal [17].

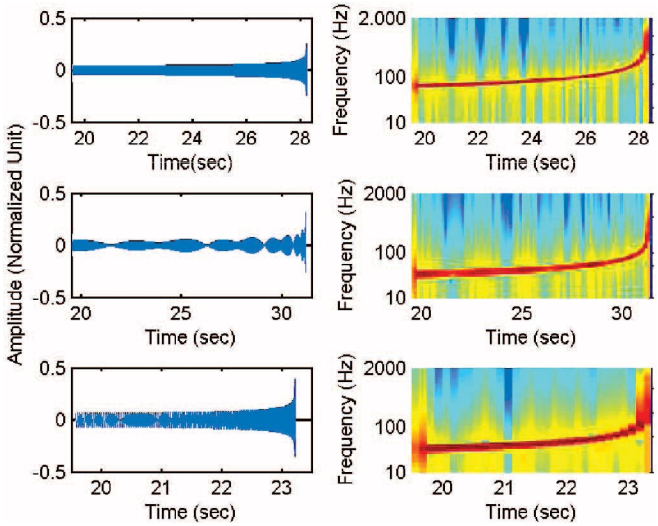

FIG. 1 (color). Examples of inspiralling gravitational waveforms (chirps) post-Newtonian order 2 at sampling frequency $f_s = 4096$ Hz from top to bottom. On the left we see the waveforms, on the right the spectrogram. Top: classical neutron star-neutron star binary $1.4M_\odot + 1.4M_\odot$; normalized units; starting frequency 60 Hz. Middle: neutron neutron star + black hole binary $1.4M_\odot + 10M_\odot$ with spinning BH; spin = 0.99; normalized units; starting frequency 30 Hz. Bottom: effective one body approach (EOB) of two inspiralling BH $5M_\odot + 10M_\odot$; normalized units; starting frequency 30 Hz.

In the following, we shall consider a (discrete time) signal with additive white Gaussian noise:

$$x_n = s_n + u_n, \tag{2}$$

where in a realistic setting the white Gaussian noise u_n can be thought of as obtained through a whitening operation of an interferometer data stream, and the signal s_n is a whitened sinusoidal signal having the form of Eq. (1).

III. AN INFINITE IMPULSE RESPONSE ADAPTIVE LINE ENHANCER FILTER

The adaptive line enhancer filter model [18] is designed to approximate the signal-to-noise ratio (SNR) gain obtained by the matched filter solution for a locally sinusoidal signal.

The advantage of using ALE filters is that no *a priori* knowledge of the signal parameters (sinusoidal frequencies, amplitudes, phases, or even the number of narrowband components) is required. Therefore, center frequency band-pass filters can be used when the signal to detect is narrow band and buried in a wide-band noise. The disadvantage of such filters is that they are only able to track a locally sinusoidal signal; therefore, if this assumption is

not verified, the tracking performance is greatly degraded. We must also consider the problem of pull-in time, i.e. the time taken by the filter to effectively track a signal and ''tune'' to its instantaneous frequency. In low signal-to-noise ratio environments, this prevents the tracking of very short signals. Such a problem can usually be addressed by running a bank of filters spanning a range of frequencies.

The most popular form of ALE is based on a finite impulse response (FIR) structure, which has the advantage of being stable and easy to adapt. However it requires a large number of adaptive weights to provide an adequate enhancement of narrow-band signals, with a consequent high computational cost [17]. Adaptive infinite impulse response (IIR) filters, instead, provide a typically narrower band with a much smaller number of weights, thus having a low computational cost; however, they are possibly subject to instabilities, and their performance surfaces are multimodal. These problems can be overcome by imposing some constraints on the filter. For line enhancement, the poles should be constrained to lay close (but inside) to the unit circle in the z plane.

In this paper, we implement the ALE as a constrained second order IIR filter with a single adaptive parameter. The general structure of the ALE is shown in the left part of Fig. 2. The purpose of the delay element is to decorrelate the input noise at the input of the filter, while leaving the response of the filter to sinusoidal excitation as unaltered as possible. The enhanced version of the sinusoid can be recovered at the output of the filter. The filter we consider has the following form, which is a reparametrization of the structure in [19] (for convenience we use the same symbol for the new parameter, i.e. w is the parameter to adapt and r is a fixed parameter determining the bandwidth of the filter):

$$H_1(z) = \frac{(1-r)(w - z^{-1})}{1 - (1+r)wz^{-1} + rz^{-2}} \tag{3}$$

with the constraints:

$$0 \ll r < 1, \qquad -1 < w < 1. \tag{4}$$

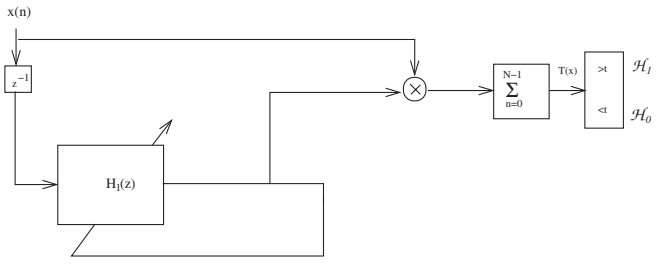

FIG. 2. Adaptive detector scheme. On the left part of the figure, schematics of the ALE filter are shown. On the right part, the detection section is shown, composed of a correlator whose output is compared with a threshold t to choose whether a signal is present ($\mathcal{H}_1$) or absent ($\mathcal{H}_0$).

With this filter structure, the processing of input sequences is performed by the filter:

$$H(z) = z^{-1}H_1(z) = \frac{(1-r)(wz^{-1} - z^{-2})}{1 - (1+r)wz^{-1} + rz^{-2}}. \tag{5}$$

The purpose of the delay element is to create the adaptive correlator structure itself. Since the filter $H_1(z)$ makes a one-step-ahead prediction of its input, we must delay the source signal $x(n)$, so that we can compare the input and output of $H_1(z)$ at the same time step to evaluate their product.

The above filter shares some analytic features with second order adaptive noise cancelers (in particular concerning poles, bandwidth, and peak location) of the general form:

$$D(z) = \frac{G(z)}{1 - 2Az^{-1}\cos\omega_0 + Bz^{-2}} \tag{6}$$

which have the following characteristics [17]:

(i) the poles form a complex-conjugate pair at angular frequency ω_0, lying on a circle of approximate radius $A \approx 1$ inside the unit circle;
(ii) the approximate 3 dB bandwidth is $(1 - B)$;
(iii) the magnitude response has a peak at angular frequency ω_0.

These characteristics in the case of the $H(z)$ filter can be read as (by comparing the denominators in Eqs. (5) and (6):

(i) The poles of the filter form a complex-conjugate pair lying on a circle of approximate radius $(1 + r)/2$ inside the unit circle.
(ii) The approximate 3 dB bandwidth is $(1 - r)$.
(iii) The magnitude response has a peak at angular frequency:

$$\omega_0 = \arccos w. \tag{7}$$

(iv) Furthermore, at the above angular frequency the filter has unity gain and zero phase shift, which guarantee that the local amplitude and phase of an input sinusoid at angular frequency ω_0 are left unaltered by the filter.

In Fig. 3 we show examples of amplitude and phase responses of the $H(z)$ filter.

The introduction of an adaptation mechanism on the w parameter has the effect of moving the peak response of $H(z)$ so as to track the instantaneous frequency of the input sinusoid. The r parameter is usually chosen close to unity to give a narrow bandwidth.

We briefly note here that this filter structure is different from the one reported in our previous works [9,10] that exhibited a magnitude response larger than 1 around the central frequency, which worsened its noise reduction capability.

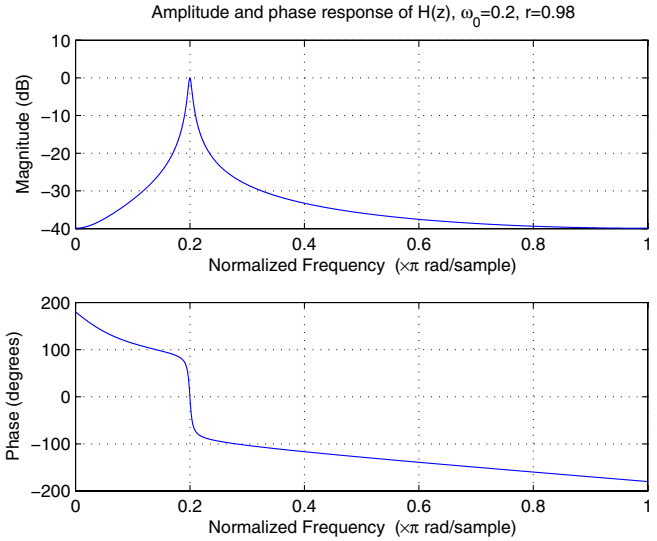

FIG. 3 (color online). Amplitude and phase response of a sample ALE filter. The phase delay at ω_0 is zero, and the amplitude response has a peak at ω_0.

A. Parameter adaptation

The output error formulation is quite natural in filtering applications [18]; however, in the case of IIR filters, in general the mean square error is not a unimodal function of the filter coefficients, thus it may have multiple minima; furthermore, filter stability during adaptation is not guaranteed.

The performance function we used for filter adaptation is the expected value of the squared filter output sequence y_n [19]:

$$\mathbb{E}[y_n^2] = |H(e^{i\omega_0})|^2 S + \frac{1-r}{1+r}\sigma^2, \tag{8}$$

where S is the (local) input signal power, σ^2 is the input noise power, and ω_0 is the instantaneous signal frequency. It can be shown that the value of w maximizing this function is given by:

$$w^* = \cos\omega_0. \tag{9}$$

The comparison of the above equation with Eq. (7) shows that the maximization of the performance function corresponds to tracking the local frequency of the input sinusoid.

An important feature of this performance function is that it is unimodal for all admissible values of w and r. This fact suggests the use of a gradient search technique to find its minimum. Following [18], we derive a normalized IIR least mean squares-type algorithm. The filter output is given by:

$$y_n = (1-r)w_n y_{n-1} - r y_{n-2} + (1-r)(w_n x_{n-1} - x_{n-2}) \tag{10}$$

so that the instantaneous estimate of the gradient is given by:

$$J = \frac{\partial y_n^2}{\partial w_n} = 2y_n \frac{\partial y_n}{\partial w_n}. \tag{11}$$

The gradient of y_n is:

$$\begin{aligned}\alpha_n &= \frac{\partial y_n}{\partial w_n} \\ &= (1+r)w_n\alpha_{n-1} - r\alpha_{n-2} + (1+r)y_{n-1} + (1-r)x_{n-1}.\end{aligned} \tag{12}$$

With these elements, we can build the parameter adaptation equation:

$$w_{n+1} = w_n + \mu y_n \alpha_n / R_{n+1}, \tag{13}$$

where R_{n+1} is an adaptive estimate of the error function Hessian [17]:

$$R_{n+1} = \nu R_n + \alpha_n^2. \tag{14}$$

The parameters μ and ν are adaptation coefficients. In the following, to ease the notation, we shall use w to denote the instantaneous value of the sequence w_n.

B. Computational cost of the adaptive correlator detector

The computational cost of the adaptive detector in Fig. 2 can be quantified by counting the number of floating point operations per sample. The relevant costs are due to the operations of the $H_1(z)$ filter (output evaluation, filter parameters adaptation), plus the product of filter input and output samples. By inspection of Eqs. (10)–(14), we have:

(i) y_n: 5 flops;
(ii) α_n: 5 flops;
(iii) w_{n+1}: 3 flops;
(iv) R_{n+1}: 3 flops.

The total cost to process a single sample (including the product of filter input and output) is therefore 17 flops. For a stream of N samples, the cost is $17N$, which can be written, using the notation for algorithmic complexity, $O(N)$, meaning that the cost of the filter operation is *linear* in the size of the data it processes. For comparison, the cost of a full matched filter analysis of a data stream is reported in [20]. As an example, for a binary coalescence of $1M_\odot + 1M_\odot$ with a SNR recovery of 90%, the computational cost is estimated to be 1.1×10^{10} flops.

C. Filter response characterization

By applying the inverse z transform to the rational function expressing the filter impulse response in the z domain, we get the time-domain impulse response:

$$\begin{aligned}h_n = \frac{2^{-n}(1-r)}{A(r,w)}[&w(C(r,w)^n - B(r,w)^n) - 2(C(r,w)^{n-1} \\ &- B(r,w)^{n-1})\theta_{n-1}],\end{aligned} \tag{15}$$

where $\theta(\cdot)$ is the unit-step function and:

$$A(r,w) = \sqrt{-4r + (1+r)^2 w^2},$$
$$B(r,w) = w + rw - A(r,w), \tag{16}$$
$$C(r,w) = w + rw + A(r,w).$$

We note that the system is strictly stable, since $h_0 = 0$.

The knowledge of the filter impulse response is necessary to characterize the output statistics of the filter. The first step to this end is the evaluation of the sample autocorrelation function g_n. It can be written as [21]:

$$g_k = \sum_{n=0}^{+\infty} h_n h_{n+k} = \begin{cases} \frac{2^{-k-1}(1-r)}{A(r,w)(1+r)}[w(1-r)(B(r,w)^k - C(r,w)^k) + -A(r,w)(B(r,w)^k + C(r,w)^k)] & k \geq 1 \\ \frac{1-r}{1+r} & k = 0 \end{cases}. \tag{17}$$

Given an input white noise sequence u_n, the autocorrelation sequence of the filter output y_n can be written as [21]:

$$\rho_k^{yy} = g_k \sigma^2, \tag{18}$$

where σ^2 is the variance of the white noise. The evaluation of the autocorrelation at lag zero gives us the expected power at the filter output:

$$\sigma_y^2 = \rho_0^{yy} = \frac{1-r}{1+r}\sigma^2, \tag{19}$$

where the factor $(1-r)/(1+r)$ is the noise reduction factor.

The cross-correlation function between the noise sequences at filter input u_n and filter output v_n can be evaluated as:

$$\rho_n^{uv} \sum_{k=0}^{+\infty} h_k \rho_{n-k}^{uu} = \sum_{k=0}^{+\infty} h_k \sigma^2 \delta_{n-k} = \sigma^2 h_n, \tag{20}$$

where we have used the fact that $\rho_{n-k}^{uu} = \delta_{n-k}$ since u is a white noise sequence. In Fig. 4 are shown the impulse response and the sample autocorrelation function in white Gaussian noise of the IIR ALE filter.

IV. ADAPTIVE CORRELATOR DETECTOR

We have seen that, due to the filter structure, for a white noise input the cross correlation between input and output at zero lag (which is a power) is exactly zero ($r_0^{uv} = \sigma^2 h_0 = 0$). In the presence of a coherent component tracked by the filter the cross correlation is going to be different from zero.

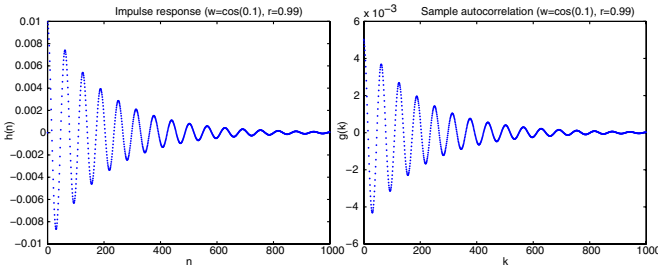

FIG. 4 (color online). Right: impulse response; Left: sample autocorrelation function.

It seems therefore natural to use an estimate of the cross-correlation function at zero lag as a detection statistic:

$$T_n = \mathbb{E}[xy] \approx \frac{1}{N} \sum_{k=n}^{n+N-1} x_k y_k = \frac{1}{N}\langle \mathbf{x}_n, \mathbf{y}_n \rangle, \tag{21}$$

where we have expressed the statistic as a stochastic process. However, for the sake of simplicity, and since we are only interested in deciding after observing nonoverlapping sequences N samples, we ignore the dependence of T from n.

It can be shown [22] that in the case of Gaussian input, T corresponds to a maximum likelihood estimate of the cross-correlation function, and that this estimate is asymptotically unbiased and consistent.

The detector would then work by comparing the value of the statistics T to a threshold t (previously set in correspondence to a desired false alarm rate) and decide that a signal is present ($\mathcal{H}_1$) if $T > t$ or absent ($\mathcal{H}_0$) if $T < t$ (also see Fig. 2).

Since a correctly tracking ALE produces estimates of the coherent components at its input, operation of the above correlator can be thought of as matched filtering of the input sequence with a noisy template signal given by the output of the ALE filter. Since ALE estimates are noisy, we can expect degraded performance with respect to a conventional matched filter operating in the hypothesis of a perfectly known signal. The main advantage is that we do not need the knowledge of a signal template.

In the next sections we shall evaluate the test statistic distributions both for the case of noise only input, and in the case of presence of signal plus noise.

A. Detection statistic distribution: Noise only

Let us consider the case where no signal is present, so that the input of the filter is a white Gaussian noise sequence, $x_n = u_n$, and the output of the filter is the correlation of the filter impulse response h_n with u_n:

$$y_n = h_n * x_n = h_n * u_n = v_n, \tag{22}$$

where $*$ is the correlation operator. The sequence v_n is Gaussian correlated noise. The test statistic can in this case be written:

$$T = \frac{1}{N}\sum_{n=0}^{N-1} x_n y_n = \frac{1}{N}\sum_{n=0}^{N-1} u_n v_n = \frac{1}{N}\langle \mathbf{u}, \mathbf{v}\rangle. \tag{23}$$

To evaluate the distribution of T, we start by considering the extended random vector $\xi = (\mathbf{u}, \mathbf{v})'$ (the prime symbol $'$ denotes the transpose operation) whose joint distribution can be derived from the marginal distributions of its components. We have $\mathbf{u} \sim \mathcal{N}(0, \sigma^2 I)$, $\mathbf{v} \sim \mathcal{N}(0, G)$, so:

$$\xi \sim \mathcal{N}\left(0, \frac{1}{N}\Sigma\right), \qquad \Sigma = \begin{pmatrix} \sigma^2 I & K \\ K' & G \end{pmatrix}, \tag{24}$$

where G is the autocorrelation matrix over a window of N samples [21], K is the cross-correlation matrix over a window of N samples [21], I is the $N \times N$ identity matrix, and "$\sim$" denotes the distribution of a random variable (Gaussian in this case).

We can express T as a quadratic form in the variable ξ by using a permutation matrix Γ:

$$T = \frac{1}{2}\xi' \Gamma \xi, \qquad \Gamma = \begin{pmatrix} 0 & I \\ I & 0 \end{pmatrix}. \tag{25}$$

The above equation is in the form of a delta-gamma-normal model, which in terms of independent variates can be written, after a change of variables (see Eq. (A1)):

$$T = \sum_{i=0}^{2N-1} \frac{1}{2}\lambda_i \zeta_i^2, \tag{26}$$

where the λ_i are the eigenvalues of the $\Gamma\Sigma$ matrix (which can be calculated, for example, by reduction to a triangular form via Schur's decomposition, and then taking the elements on the diagonal).

It should be noted that since the filter used in the analytical derivation of the T distribution is not adaptive, we must assess if (and how much) filter adaptivity alters the theoretical derivation. We shall show by a statistical test that the analytical derivation is not affected in a significative way.

In Fig. 5 we show the empirical and model distributions of T. The former is evaluated through the direct operation of the adaptive detector on white noise sequences, the latter is obtained by sampling the model distribution given by Eq. (26) (which assumes a static filter). The difference ΔF between the statistics is also shown, to give a better idea of the goodness of the model.

For the case in figure, a two-sided Kolmogorov-Smirnov test [23] shows that the null hypothesis that the two distributions are equal cannot be rejected at significance level 0.05. The Kolmogorov distance between the two distributions is 2.8×10^{-3}.

While for evaluation of the detector performance numerical Fourier inversion can be used, in a practical operation of the detector we only need to calculate the threshold corresponding to a prescribed false alarm probability α, which is the $(1 - \alpha)$-quantile of the distribution of

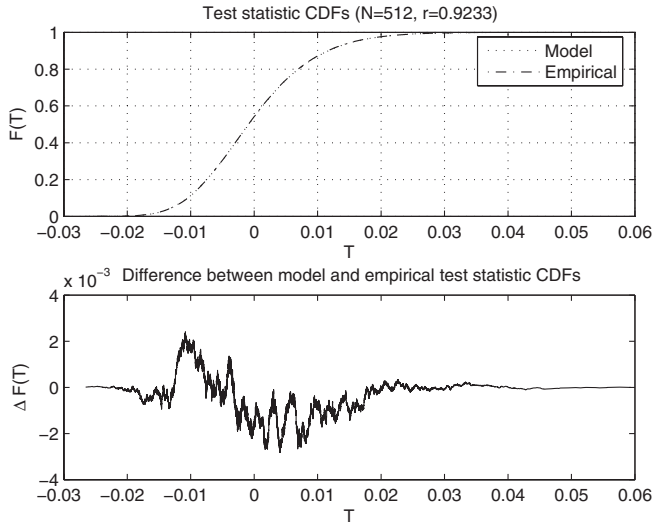

FIG. 5. Example of the adaptive detector output statistics distribution (model and empirical). Their difference is also shown.

T [24]. Since this is typically small, it can be accurately evaluated from an asymptotic expansion of the right tail of the distribution of T. In Appendix B, by following the approach in [25], we show a closedform expression to evaluate the detection threshold for a prescribed false alarm probability α.

An essential element for the approximation is the evaluation of the eigenvalues spectrum of the $\Gamma\Sigma$ matrix; this problem, however, for large values of N can be computationally very intensive. Although the eigenvalues must be evaluated only once for a given filter structure (defined by bandwidth and starting frequency N), it may be necessary to define different filter structures, for example to create an array of filters operating in parallel at different starting frequencies.

In general, it is difficult to say how the filter parameters affect the eigenvalue spectrum (and, as a consequence, the threshold). However, simulations can be used to have an empirical insight into the problem. As an example, in Fig. 6 we show how the choice of the bandwidth affects the threshold, given false alarm probability (hereinafter P_{fa}), sampling frequency, and N. For a given P_{fa}, the threshold increases with the bandwidth B. A higher threshold, however, means that the detection probability decreases, so one should use as low a threshold as possible, which implies a low bandwidth. But a very low bandwidth reduces the tracking capabilities of the filter. It is therefore clear that there is a trade off between bandwidth and detection capability.

These kind of analyses could be used to fit a regression model, which, given as inputs the filter bandwidth, the false alarm probability, and N, gives an approximate value of the threshold. We are currently working on a neural network-based regression model.

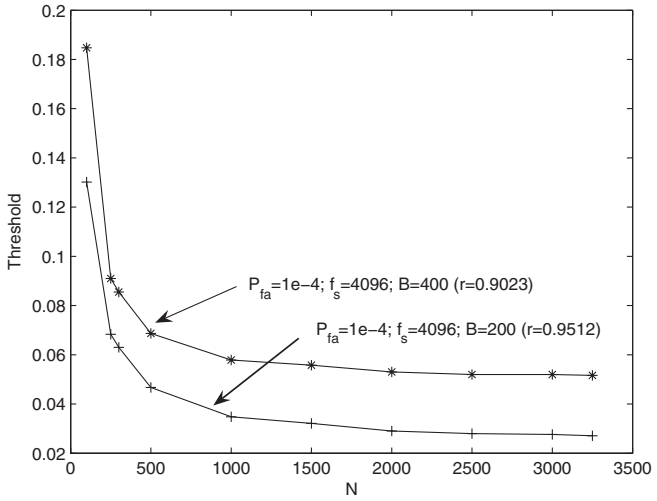

FIG. 6. Relation between bandwidth (B) and threshold, given false alarm probability (P_{fa}), sampling frequency (f_s), and N.

B. Detection statistic distribution: Signal plus noise

In the case in which a signal is present, $x_n = s_n + u_n$ and the output of the filter is given by Gaussian correlated noise with an added signal component:

$$y_n = h_n * x_n = h_n * [s_n + u_n] = h_n * s_n + \upsilon_n = \hat{s}_n + \upsilon_n. \tag{27}$$

The test statistic can in this case be written:

$$T = \frac{1}{N}\sum_{n=0}^{N-1} x_n y_n = \frac{1}{N}\sum_{n=0}^{N-1}[s_n + u_n][\hat{s}_n + \upsilon_n]. \tag{28}$$

If the ALE filter is correctly tracking the signal, so that it does not introduce a phase delay and its magnitude is approximately one, we can assume that $s_n \approx \hat{s}_n$, so we can write:

$$\begin{aligned} T &= \frac{1}{N}\sum_{n=0}^{N-1} x_n y_n = \frac{1}{N}\sum_{n=0}^{N-1}[s_n + u_n][s_n + \upsilon_n] \\ &= \frac{1}{N}\sum_{n=0}^{N-1} s_n^2 + \frac{1}{N}\sum_{n=0}^{N-1} s_n[u_n + \upsilon_n] + \frac{1}{N}\sum_{n=0}^{N-1} u_n \upsilon_n \\ &= \mathcal{E} + \frac{1}{N}\langle \mathbf{s}, \mathbf{u} + \mathbf{v}\rangle + \frac{1}{N}\langle \mathbf{u}, \mathbf{v}\rangle, \end{aligned} \tag{29}$$

where $\mathcal{E} = \mathbf{s}'\mathbf{s}/N$ is a quadratic measure of the signal power. If we introduce the *signal vector* $\Delta = \frac{1}{\sqrt{N}}(\mathbf{s}, \mathbf{s})'$, so that $\frac{1}{N}\langle \mathbf{s}, \mathbf{u} + \mathbf{v}\rangle = \Delta'\xi$, we have:

$$T = \mathcal{E} + \Delta'\xi + \tfrac{1}{2}\xi'\Gamma\xi \tag{30}$$

which is a quadratic form (see Appendix A). So, the presence of a signal is reflected in the formal expression for the case of noise only, by additional constant and linear terms in ξ.

C. Comparison with matched filter detector

It is instructive to briefly compare the detection statistic of the ALE correlator detector, with the detection statistic of the matched filter. It is well known [26] that the latter can be written:

$$T_M = \sum_{n=0}^{N-1} x_n s_n = \langle \mathbf{x}, \mathbf{s}\rangle, \tag{31}$$

where, as before, $\mathbf{x}$ is the observed data, and $\mathbf{s}$ is the (known) signal vector (*template*). This expression shows that the detection statistic is a *linear form* in the data, while the detection statistic for the ALE detector in Eq. (30) is a *quadratic form* in the data. Therefore the detectors are essentially different, notwithstanding the fact that at the highest level the two detectors work based on the same principle.

V. SIMULATION RESULTS

In all large baseline laser interferometric GW antennas output data, starting from the 40 m Caltech interferometer and going to VIRGO, LIGO, GEO, and TAMA, many relevant effects are present. Violin resonances in the suspensions, main power harmonics, ring-down noise from servo control systems, electronic noises, transients, non-Gaussianity, nonstationarity, and nonlinearity of the dark fringe data are common features of the measured noise. Our goal is to assess the performance of IIR ALE, thus we must evaluate, taking into account the experimental noise, what will be the behavior of IIR ALE as GW receiver both in white noise and in not perfectly whitened noise. To this aim we performed simulations using realistic Virgo-like data segments, whitened by using a linear autoregressive filter with 16 384 coefficients estimated with Burg's algorithm [17]. The complexity of the model was estimated by statistical cross validation [27]. The number of parameters in a model is a measure of its complexity. As the number of parameters increases, a model will be able to better approximate the data it is fitted on. However, this does not guarantee that the same model will perform equally well on data it has never seen before; the model will act as an interpolator, rather than a regressor. Therefore, it is necessary to control the model complexity, and cross validation is a statistical technique that allows such a control. In practice, a range of models with different number of parameters is fitted on a block of data, and its performance is tested on a different block of data. The prediction performances of all models are evaluated on this new block, and the model with the best performances is chosen as the reference model.

Finally, to assess the influence of nonstationarities and incorrect whitening, we evaluated the decision statistics for different noise sources.

A. Simulation in white noise

In this section we will show the simulated tracking performances of IIR ALE for varying frequency of input sinusoid in white noise, such that the corresponding frequency variation is a frequency step. The simulations were performed with the following specifications of the input and the filter: for $0 \leq t \leq 0.5$ sec, $f = 180$ Hz and for $0.5 < t \leq 1$ sec, $f = 220$ Hz; amplitude $A = \sqrt{2}$; sampling frequency $f_s = 4096$ Hz; SNR = 26.5; filter parameters $\mu = 0.1$, $\nu = 0.97$, $r = 0.97$, $R_0 = 10\,000\,000$. Before the occurrence of the step, care is taken to ensure that the adaptive filter is in steady state, by considering near steady state initial conditions and allowing sufficient time i.e. at least 1000 samples. In Fig. 7 there are shown the results of the simulation. In Fig. 7 (top left) there is shown the theoretical frequency response (dotted curve) vs time and the simulated mean response (blue curve) embedded in the standard error curves; these are computed on 2000 realizations of the simulation. The signal is corrupted by white noise of zero mean and variance $\sigma^2 = 6.25$. From the frequency step response it is clear that there is a delay of about 0.1 sec for the filter to adapt as it is also possible to see in Fig. 7 (bottom left) where it is shown the amplitude residuals (vs time), between the tracked signal and the theoretical one. We must note that from the output of the filter we can extract two kinds of information in real time that is either the output amplitude or the frequency of the tracked signal (if any) at the input. In Fig. 7 (top right) there is shown the noisy input and in red the output of IIR ALE. In Fig. 7 (bottom right) there are shown the linear SNR for each of the 2000 noise realizations. The red lines represent the mean SNR (26.5) embedded in the standard

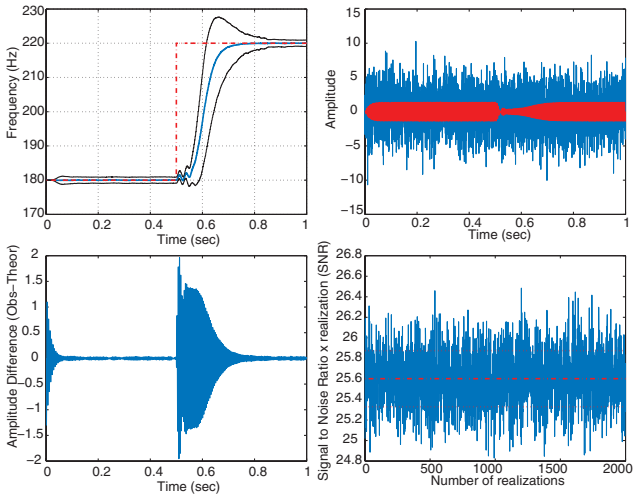

FIG. 7 (color). Frequency step from 180 Hz to 220 Hz applied in a sinusoidal signal of amplitude $\sqrt{2}$ and duration 1 sec at sampling frequency $f_s = 4096$ Hz embedded in white noise (SNR = 26.5). The parameter of IIR ALE were $\mu = 0.1$, $\nu = 0.97$, $r = 0.97$, $R_0 = 10\,000\,000$.

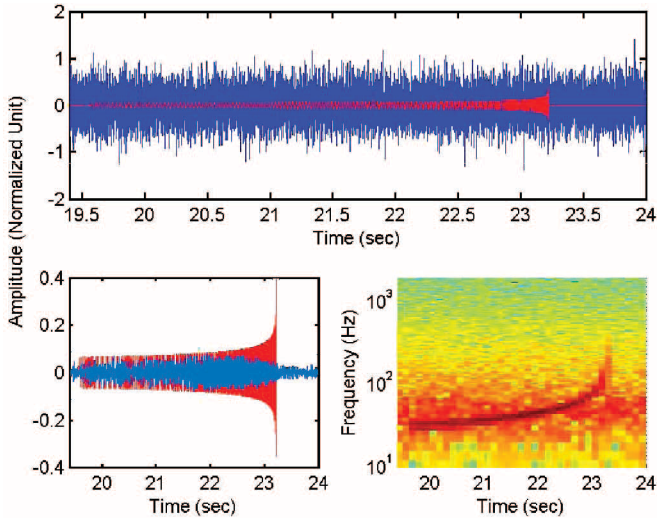

FIG. 8 (color). Examples of inspiralling gravitational waveforms (chirps) at sampling frequency $f_s = 4096$ Hz. Top: neutron star + black hole binary $5M_\odot + 10M_\odot$, in normalized units, waveform computed by effective one body (EOB) approach; starting frequency 30 Hz, embedded in white noise (SNR = 20). Bottom left: theoretical waveform (red) and detected waveform (blue). Bottom right: time-frequency behavior of the detected waveform by IIR ALE.

SNR error. In the following, we also show three examples of simulated chirp detections in white noise:

(i) $1.4M_\odot + 1.4M_\odot$ Binary inspiralling towards the merger phase, post-Newtonian order 2.5, normalized units, embedded in white noise with SNR 24.5, sampling frequency of 4096 Hz and starting frequency of 60 Hz.

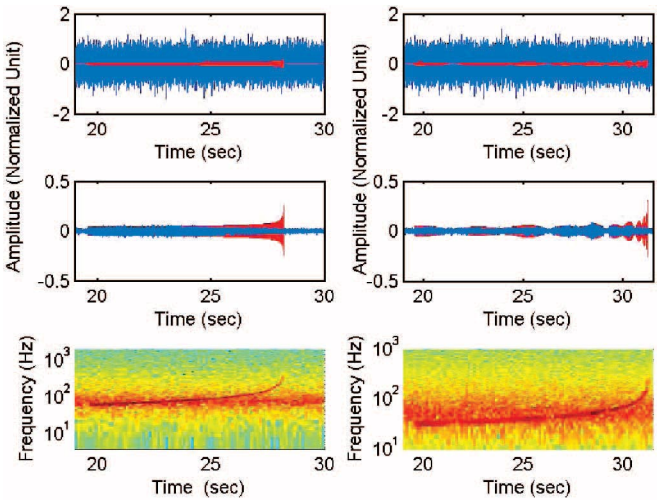

FIG. 9 (color). Examples of inspiralling gravitational waveforms detection at sampling frequency $f_s = 4096$ Hz. Top left: classical neutron star-neutron star binary $1.4M_\odot + 1.4M_\odot$ in normalized unit with starting frequency 60 Hz, embedded in white noise (SNR = 24.5).

(ii) $1.4M_\odot + 10M_\odot$ Binary-spinning BH post-Newtonian order 2 embedded in white noise with SNR 20, sampling frequency of 4096 Hz, starting frequency of 30 Hz, BH Spin = 0.99 (Fig. 8).

(iii) $5M_\odot + 10M_\odot$ Black hole-black hole (BH) effective one body (EOB) approach post-Newtonian order 2 embedded in white noise with SNR 20, sampling frequency of 4096 Hz and starting frequency of 30 Hz (Fig. 9).

As shown in Figs. 8 and 9, the promising characteristic of this kind of trigger is also the possibility to have an insight of the waveform amplitude and of the time-frequency behavior. The weak point is connected with the loss in amplitude of the final part of the chirp, due to the nonadiabatic behavior of the frequency evolution. Nonetheless the frequency variation is nearly tracked, as it is possible to see from the time-frequency diagrams.

B. Test statistics for colored and nonstationary noise sources

We evaluated how much possible nonstationarities and imperfect whitening of real interferometric noise impact on the performance of the adaptive detector. In particular, we assessed the influence of nonwhite noise sources on the detection threshold. Since it is difficult to analytically evaluate such effects, we used extensive Monte Carlo simulation runs. For each experiment, we used 1.300.000 samples; such a choice guarantees that the smallest probability which can be evaluated is 0.05, and that the relative error e in the probability estimate satisfies:

$$P(|e| > 0.01) \leq 0.01 \tag{32}$$

which means that e is larger than 0.01 (in absolute value) with probability at most 0.01 [26].

The first test involves an autoregressive moving average (ARMA) process of second order, fed by white Gaussian noise with unity variance. The power spectral density of the process is shown in Fig. 10.

The second test involves the same process as above, but its amplitude is modulated in time by the function $n^{1/4}$, where n is the discrete time index. The process obtained is nonstationary, and its probability density is non-Gaussian and leptokurtotic (i.e. more peaked than a Gaussian probability density).

Figure 11 shows the simulated test statistic for the above noise sources; comparing also the test statistic for white Gaussian noise.

Since the ALE is designed to track slowly varying sinusoids, it is not able to exactly track the spectral features of the above noise sources. However, this influences the filter response, and consequently the test statistic distribution. As it clearly appears from Fig. 11, for a given detection threshold there is a large increment in the false alarm probability. For example, for a threshold $T = 0.05$, the false alarm probability in the white Gaussian case is $\approx$

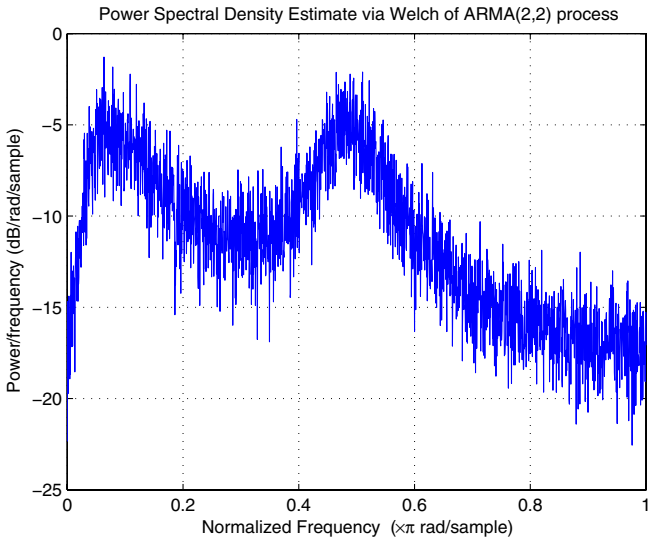

FIG. 10 (color online). Power spectral density of colored ARMA (2,2) process used as noise source.

10^{-11}, while for the ARMA and nonstationary cases they are ≈ 0.42 and ≈ 0.91, respectively. So, there is a large loss in efficiency, depending on the increasing nonstationarity of the noise sources and the residual colored noise after the whitening procedure. The main effect is an increase in the false alarm rate.

Figure 12 shows receiver operating characteristic (ROC) curves for the proposed adaptive matched filter. ROC curves compactly describe the performances of a detector, in terms of the relationship between false alarm and detection probabilities. There is a natural trade off between these two quantities, since by incrementing the probability of detection, we also increment the probability of false detections.

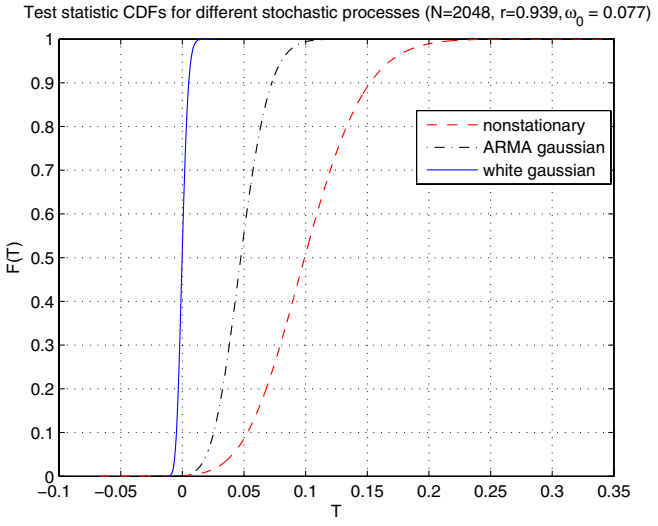

FIG. 11 (color online). Empirical test statistic distributions for different noise sources.

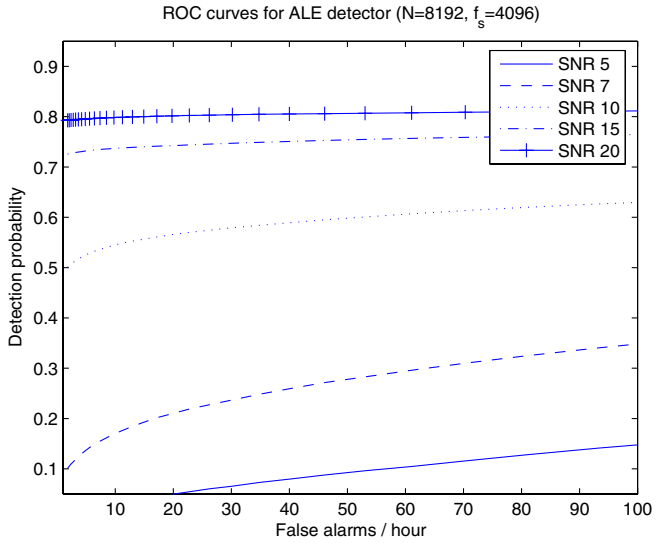

FIG. 12 (color online). Receiver operating characteristics for ALE detector with whitened input. The SNR ranges from 5 to 20.

We embedded a chirp signal (post-Newtonian order 2.5, chirp mass 1.4, lower cutoff frequency 50 Hz, sampling frequency $f_s = 4096$ Hz) in simulated Virgo noise, then whitened the resulting sum. The whitened data were then fed to an ALE matched filter with an integration time of $N = 8192$ samples (corresponding to two seconds). The SNR ranges from 5 to 30. It should be noted that these SNRs refer to the whole chirp (whose length is 44 532 samples). The ALE works only on 8192 samples, so the effective SNR "seen" by the filter is just a fraction of the total SNR which could be obtained by using the full signal. Since the chirp amplitude is growing, tracking is easier towards the final stages of signal evolution, so we can expect a large contribution to the detection coming from these stages. However, as we have shown in the simulations, when the signal frequency becomes too steep, ALE is not able to track it anymore.

Since the adaptive filter operates starting from a fixed frequency, in actual use of the filter it is conceivable to use an array of filters starting from different frequencies to process data. Work is under way to characterize the decision statistics of this multifilter structure. We can conclude that the performances of the IIR ALE filters are encouraging by using them as a first level trigger to isolate interesting segments of data for further analysis with matched filters.

VI. CONCLUSION

In this work we have extended our previous results on the use of ALE filters for GW detection. We have defined an adaptive matched filter structure, in which a noisy template probability (if a signal is present), is adaptively built by the ALE, whose output is then fed to a correlator detector. The theoretical adaptive matched filter performance characteristics have been evaluated and compared with the classic matched filter's ones. The performance loss in terms of probability of detection has been shown not to be excessive under the hypothesis of white Gaussian noise; the performance loss is balanced by the low computational cost of the filter. This adaptive matched filter structure (IIR ALE + correlator) can be a useful first level trigger to select interesting data segments to be later analyzed by use of classic matched filter-based techniques. IIR ALE is not useful for very short signals, like GW bursts, due to the response time of the filter. It could be useful for GW signal from pulsars, but the intrinsic weakness of those kind of signals rules out any practical use.

APPENDIX A: THE DELTA-GAMMA-NORMAL FAMILY OF MODELS

To evaluate the detection performance of the proposed detector, the distribution of the test statistic T must be computed. As we shall see, this problem is not an easy task, since the distributions we get cannot be expressed in closed form. In particular, we shall show that after suitable algebraic manipulation the test statistic can be written as a quadratic form in normal variates ξ:

$$T = \theta + \Delta'\xi + \tfrac{1}{2}\xi'\Gamma\xi. \tag{A1}$$

This model is termed delta-gamma-normal [25,28].

To ease analytical treatment of the statistic T, we must write it as a sum of independent random variates that are functions of standard normal random variables ζ_i. This can be done by solving the generalized eigenvalue problem, i.e. finding matrices C and Λ such that:

$$CC' = \Sigma, \qquad C'\Gamma C = \Lambda. \tag{A2}$$

By defining:

$$\xi = C\zeta, \qquad \delta = C'\Delta, \qquad \Lambda = \mathrm{diag}(\lambda_0, \ldots, \lambda_{N-1}) \tag{A3}$$

we can write:

$$T = \theta + \sum_{i=0}^{2N-1}\left[\delta_i\zeta_i + \frac{1}{2}\lambda_i\zeta_i^2\right]. \tag{A4}$$

APPENDIX B: ASYMPTOTIC TAILS AND QUANTILES

Let the generalized eigenvalues of T in Eq. (26) be sorted in increasing order. Suppose there are $M \leq 2N$ distinct eigenvalues, and let i_j be the highest index of the jth distinct eigenvalue, and μ_j be its multiplicity. We have then $\lambda_{i_1} < \lambda_{i_2} < \ldots < \lambda_{i_M}$. For $j = 1, \ldots, M$, define:

$$T_j = \frac{1}{2}\lambda_{i_j}\sum_{l=i_{j-1}+1}^{i_j}\zeta_l^2 \tag{B1}$$

then the T_j are independent, and we have:

$$T = \sum_{j=1}^{M} T_j. \tag{B2}$$

The above equation essentially defines T as a sum of independent χ^2 random variables with different degrees of freedom and scales. Specifically, if $g(\cdot;\mu_j)$ is the $\chi^2_{\mu_j}$ density, then the density of T_j is:

$$f_j(x) = \frac{2}{|\lambda_{i_j}|} g\left(\frac{2}{\lambda_{i_j}} x;\mu_j\right). \tag{B3}$$

Since we are interested in the upper quantiles of the distribution of T, according to the results in [25] we should distinguish three cases, based on the sign of the largest eigenvalue. However, in our case it is possible to show that *the largest eigenvalue of the* $\Gamma\Sigma$ *matrix is always positive*. In fact the Γ matrix acts on Σ with a block permutation:

$$\Gamma\Sigma = \frac{1}{N}\begin{pmatrix} K' & G \\ \sigma^2 I & K \end{pmatrix}. \tag{B4}$$

It is possible to show that [21]:

$$\mathrm{Tr}\,(\Gamma\Sigma) = 2\sigma^2 h_0 = 0. \tag{B5}$$

Since for every square matrix the sum of its eigenvalues equals its trace, we have:

$$\sum_{i=1}^{N} \lambda_i = 0, \tag{B6}$$

where λ_i are the eigenvalues of $\Gamma\Sigma$. Excluding the degenerate case in which all eigenvalues are zeros (since in this case, by Eq. (B2), we would get a degenerate density), then we have both positive, negative, and zero eigenvalues, such that their sum is zero. Therefore, there must exist at least one positive eigenvalue (possibly of multiplicity greater than one) which is largest. So, we are allowed to consider only the case in which the largest eigenvalue is positive.

We can now apply the following result from [25]. Let $\alpha \to 0$, then the upper quantile of T satisfies the following equation:

$$x_{1-\alpha} = \lambda_{i_M} \ln b_M + \frac{\lambda_{i_M}}{2}\chi^2_{1-\alpha,\mu M} + O(1/\sqrt{\chi^2_{1-\alpha,\mu M}}), \tag{B7}$$

where $\chi^2_{1-\alpha,\mu_M}$ is the $(1-\alpha)$-quantile of the $\chi^2_{\mu_M}$ distribution and:

$$b_M = \prod_{j=1}^{M-1}\left(1 - \frac{\lambda_{i_j}}{\lambda_{i_M}}\right)^{-\mu_j/2}. \tag{B8}$$

It should be noted that in practice the false alarm probability must be smaller than 10^{-2} for the approximation to hold.

[1] C. W. Misner, K. S. Thorne, and J. A. Wheeler, *Gravitation* (Freeman, San Francisco, 1973).
[2] D. G. Blair, *The Detection of Gravitational Waves* (Cambridge University Press, Cambridge, England, 1991).
[3] P. R. Saulson, *Fundamentals of Interferometric Gravitational Wave Detectors* (World Scientific, Singapore, 1994).
[4] F. Acernese *et al.*, Classical Quantum Gravity **21**, S385 (2004).
[5] D. Sigg, Classical Quantum Gravity **21**, S409 (2004).
[6] B. Willke *et al.*, Classical Quantum Gravity **21**, S417 (2004).
[7] R. Takahashi (TAMA Collaboration), Classical Quantum Gravity **21**, S403 (2004).
[8] P. Bender, I. Ciufolini, J. Cornelisse, K. Danzmann, W. Folkner, F. Hechler, J. Hough, Y. Jafry, R. Reinhard, D. Robertson, A. Rü diger, M. Sandford, R. Schilling, B. Schutz, R. Stebbins, T. Summer, P. Toubol, S. Vitale, H. Ward, and W. Winkler, ESA Pre-Phase A Report, Max Planck Institut für Quantenoptik Report No. MPQ 208, 1996.
[9] L. Milano, F. Barone, and M. Milano, Phys. Rev. D **55**, 4537 (1997).
[10] F. Acernese, F. Barone, R. De Rosa, A. Eleuteri, and L. Milano, Classical Quantum Gravity **21**, S781 (2004).
[11] Eanna E. Flanagan and Scott A. Hughes, Phys. Rev. D **57**, 4566 (1998).
[12] M. Campanelli, C. O. Lousto, P. Marronetti, and Y. Zlochower, Phys. Rev. Lett. **96**, 111101 (2006).
[13] F. Pretorius, Phys. Rev. Lett. **95**, 121101 (2005).
[14] A. Buonanno and T. Damour, Phys. Rev. D **62**, 064015 (2000).
[15] P. Ajith, B. R. Iyer, C. A. K. Robinson, and B. S. Sathyaprakash, Phys. Rev. D **71**, 044029 (2005).
[16] A. Buonanno, Y. Chen, Y. Pan, H. Tagoshi, and M. Vallisneri, Phys. Rev. D **72**, 084027 (2005).
[17] S. Haykin, *Adaptive Filter Theory* (Prentice-Hall, Englewood Cliffs, NJ, 1995).
[18] B. Widrow and S. Stearns, *Adaptive Signal Processing* (Prentice-Hall, Englewood Cliffs, NJ, 1985).
[19] D. R. Hush *et al.*, IEEE Trans. Acoust. Speech Signal Process. **34**, 1380 (1986).
[20] P. Canitrot, L. Milano, and A. Vicere, VIRGO Report No. VIR-NOT-PIS-1390-149, 2000.

[21] A. Oppenheim and R. W. Schafer, *Digital Signal Processing* (Prentice-Hall, Englewood Cliffs, NJ, 1975).

[22] S. Kay, Fundamentals of Statistical Signal Processing, Vol. I, *Estimation Theory* (Prentice-Hall, Englewood Cliffs, NJ, 1998).

[23] A. Papoulis, *Probability, Random Variables and Stochastic Processes* (McGraw-Hill, New York, 1992), 3rd ed.

[24] J. Abate and W. Whitt, Queueing Systems, Theory and Applications **10**, 5 (1992).

[25] S. Jaschke, C. Klüppelberg, and A. Lindner, J. Multivariate Anal. **88**, 252 (2004).

[26] S. Kay, Fundamentals of Statistical Signal Processing, Vol. II, *Detection Theory* (Prentice-Hall, Englewood Cliffs, NJ, 1998).

[27] K. Fukunaga, *Introduction to Statistical Pattern Recognition* (Academic, New York, 1990), 2nd ed.

[28] N. N. Vakhaniya and N. P. Kandelaki, Soobshcheniia Akademii nauk Gruzinskoi SSR **50**, 535 (1968) (in Russian).